Solid-State Defect Mechanism in Vanadyl Pyrophosphate Catalysts: Implications for Selective Oxidation

Pratibha L. Gai* and K. Kourtakis

High-resolution and in situ electron microscopy of vanadyl pyrophosphate catalysts reacted in alkane (*n*-butane) and other reducing environments have shown evidence for surface structure modifications accompanied by two sets of symmetry-related extended defects. Defect analysis reveals that the defects are formed by pure (glide) shear mechanism. The defect mechanism suggests the presence of basal (coplanar) anion vacancies, associated with Lewis acid centers, at oxygen sites linking corner-sharing phosphorus tetrahedra and vanadyl octahedra in the active plane. These in-plane defect sites may be key to the activation of the alkane, especially in the dehydrogenation.

Complex vanadium-phosphorus oxide heterogeneous catalysts are used industrially for the partial oxidation of alkanes (*1–6*). In the selective oxidation of *n*-butane to maleic anhydride (MA) the "best active phase" has been identified as the vanadyl pyrophosphate, $(VO)_2P_2O_7$ (VPO), with active centers located at the exposed (010) planes (*3–10*). This phase is usually prepared by the calcination of a precursor phase, the hemihydrate, $(VO)HPO_4{\cdot}0.5\ H_2O$ (*1–11*), by a topotactic dehydration mechanism (*6*).

Preparative procedures for the catalysts have a marked effect on their activity (*9–11*). The active phases are produced either (i) in organic media [reduction of V_2O_5 with isobutyl alcohol and addition of orthophosphoric acid (*12*)]; (ii) in aqueous media [reduction of V_2O_5 and HCl, with orthophosphoric acid and water (*13*)] or (iii) by the reduction of $VOPO_4$ through the formation of crystallographic shear (CS) planes (*4*). For high-performance catalysts (capable of activating *n*-butane), the route that uses organic media, which results in a large area of active (010) faces, is generally chosen; the other methods of preparation can be multiphasic, which would modify the reactivity of the catalyst (*4, 6, 9, 13*). The calcined catalysts are thought to contain mixed valance V^{V}–V^{IV} pairs (*10*), and x-ray diffraction of single crystals has shown disorder of the vanadium (*14*).

The selectivity and activity of a working catalyst depends very strongly on its microstructure. However, microstructural modifications (disordered structure) of the pyrophosphate catalyst in selective oxidation of butane to MA are not well understood. We have obtained insights into the solid-state reaction mechanisms by examining the catalyst microstructures in butane and in other environments.

We prepared gray powders of VPO by the organic route, using vanadium pentoxide and anhydrous phosphoric acid in isobutyl alcohol and benzyl alcohol (*9*). Catalyst reactivity tests were performed at ~400°C in a fluidized bed reactor, in butane and alternatively in a butane-air mixture, in H_2, and in N_2. Samples were reacted for durations ranging from ≤ 1 hour to several days. Changes in the surface of the catalyst were observed by selected-area electron diffraction (SAED) and high-resolution electron microscopy (HREM). For HREM at the atomic level and for in situ electron microscopy in controlled atmospheres, a modified Philips CM30 high-resolution electron microscope (*15, 16*) fitted with an environmental cell (to allow direct observations in a controlled gas environment at various temperatures) was used. It has a lattice resolution of ~2 Å and is integrated with energy-dispersive x-ray (EDX) analysis for simultaneous microchemical characterization. We also carried out detailed studies of the image contrast in this electron microscope, by tilting the catalyst to various Bragg reflecting conditions (*17, 18*). Samples were very electron beam–sensitive, and experimental conditions similar to those used in zeolite imaging (*19*) were imposed.

An idealized structural model of VPO (*4–8*) in (010) projection is shown in Fig. 1A. The crystalline lattice consists of vanadyl pairs with the V coordination shaped in distorted edge-shaped octahedra, which are connected to each other by phosphate tetrahedra to form infinite layers.

It is believed (*4–6*) that the (010) basal plane is active for butane oxidation, and various suggestions on the nature of active sites have been made. Variable formal oxidation states (~3.7 to 4.4, based on bond-strength calculations) are thought to exist in the pairs of the neighboring V atoms, facilitating electronic interactions between them. Assuming trans-disposition of V=O in the octahedral pairs, an anion vacancy on top of one V is suggested (*4, 6, 13*). Butane requires strong acid sites for dehydrogenation, and $V^{3.7+}$ or $V^{4.4+}$ located near such oxygen sites is believed to be capable of abstracting the hydrogen groups. However, controlled environmental in situ EM studies of CS defect structures (*20*) have shown that a CS plane (which eliminates vacant anion sites and causes structural collapse to a lower energy configuration), once formed, is a low-energy plane; a CS plane that is also a cleavage plane, as in the case of (010), is expected to have a coordinatively saturated stable configuration in the ordered equilibrium state. The studies also indicated that anion vacancies are active centers for fast oxygen diffusion; CS planes are not active centers.

In Figs. 2 and 3, we present SAED and HREM images of VPO before and after the reaction with butane at 400°C, respectively. The atomic structure image of a fresh VPO catalyst in (010) planar projection is shown in Fig. 2A, with the structural model (from Fig. 1A) approximately superimposed, to elucidate the V and P atom columns. The SAED is shown in Fig. 2B. A contrast simulation at Scherzer defocus was used to verify the positioning of the model.

The butane-reduced crystals showed two sets of extended defects in diffraction contrast and in HREM (Fig. 3, A and C, respectively) in the (020) cleavage plane. The two sets of defects were found to be along symmetry-related ⟨201⟩ directions in this plane and occurred with equal probability along [201] and [20$\bar{1}$]. The corresponding electron diffraction pattern (Fig. 3B) indicates streaking (disorder) along these two directions. Diffraction contrast analyses, obtained by tilting the crystal to various Bragg reflections including 201 and 20$\bar{1}$ reflections (Fig. 4, A and B), have indicated that the shear or the displacement vector **R** of the defects lies in the plane of shear [that is, the defects are formed by pure (homogeneous or translational glide) shear], creating {201} fault planes. The magnitude of **R** was found from the defect analyses to be ~3 Å, with **R** approximately of the type $\pm \langle a/7, 0, c/4 \rangle$. The defects nucleated initially at the surface and extended into the bulk within a few minutes. The defect concentration increased with time, extending throughout the bulk in several hours, and the samples were covered with defects after a few days.

We confirmed the formation of the defects by dynamic studies of the reduction of the catalyst by N_2 in an electron microscope fitted with an environmental cell.

DuPont Science and Engineering Laboratories, Central Research and Development, Wilmington, DE 19880, USA.

*To whom correspondence should be addressed.

These defects observed in situ and the defects present in samples reacted ex situ in the fluidized bed reactor in N_2 were identical to those observed in butane, ruling out any hydroxide formation. The defect density in N_2 (and in H_2) was lower than that in butane at the same temperature. In a butane-air mixture, the extended defect density was greatly reduced; we believe that this may be due to the reoxidation of at least some of the defects upon exposure to gas-phase O_2.

The diffraction contrast image analysis has shown that the extended defects are formed by a pure shear mechanism that generates {201} type pure shear planes, or antiphase boundaries. If we ignore the distortion in the octahedra, the nature of these planar stacking faults in one layer of the idealized VPO structure is shown in a model in Fig. 1B. The shear defect model indicates that some of the oxygen atoms along ⟨201⟩ are lost during reduction. A schematic of the faults along ⟨201⟩ is shown in Fig. 1C. The faults increase in density and begin to order as a function of time, resulting in the growth of the (201) face at the expense of the (010) face. This is consistent with the calculations that (201) is a lower energy surface than (010) (*21*).

Because these extended defects are observed only in reduction environments as a result of the gas-catalyst interactions, we believe that they arise as a result of the reduction of VPO by the loss of lattice oxygen ions. The SAED patterns show diffuse streaking (disorder) after the reduction of VPO.

We propose the following explanation for the extended defects and the associated disorder observed along the symmetry-related ⟨201⟩ in SAED. Under the reducing conditions, there is a large driving force for the generation of anion vacancies. A high concentration of anion vacancies is introduced into the crystal by reduction at the catalyst surface, and these vacancies diffuse into the crystal. To provide the minimization of the accompanying strain energy, the crystal simply glides along ⟨201⟩ directions

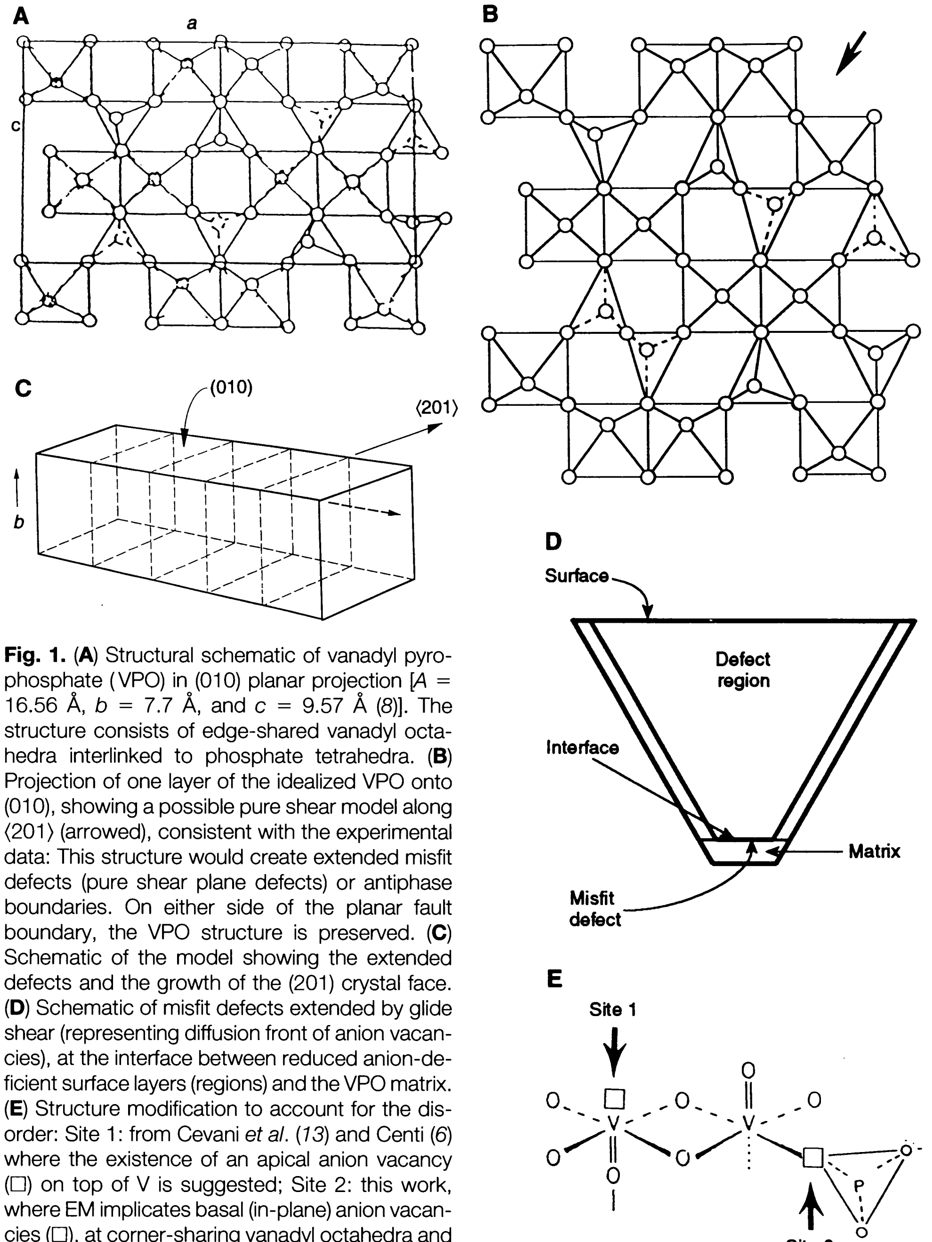

Fig. 1. (**A**) Structural schematic of vanadyl pyrophosphate (VPO) in (010) planar projection [A = 16.56 Å, b = 7.7 Å, and c = 9.57 Å (*8*)]. The structure consists of edge-shared vanadyl octahedra interlinked to phosphate tetrahedra. (**B**) Projection of one layer of the idealized VPO onto (010), showing a possible pure shear model along ⟨201⟩ (arrowed), consistent with the experimental data: This structure would create extended misfit defects (pure shear plane defects) or antiphase boundaries. On either side of the planar fault boundary, the VPO structure is preserved. (**C**) Schematic of the model showing the extended defects and the growth of the (201) crystal face. (**D**) Schematic of misfit defects extended by glide shear (representing diffusion front of anion vacancies), at the interface between reduced anion-deficient surface layers (regions) and the VPO matrix. (**E**) Structure modification to account for the disorder: Site 1: from Cevani *et al.* (*13*) and Centi (*6*) where the existence of an apical anion vacancy (□) on top of V is suggested; Site 2: this work, where EM implicates basal (in-plane) anion vacancies (□), at corner-sharing vanadyl octahedra and phosphate tetrahedra.

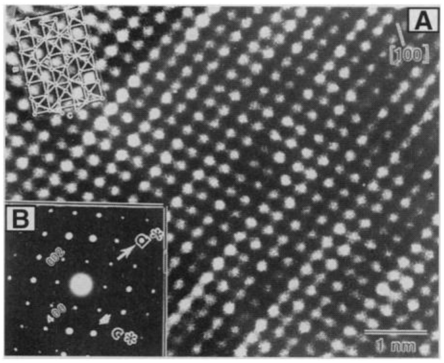

Fig. 2. (**A**) The HREM atomic structure image of the fresh VPO catalyst in the (010) plane. (**B**) The SAED pattern. The structural model (in Fig. 1A) is approximately superimposed to elucidate atomic columns, with dark regions corresponding to columns of P and V atoms.

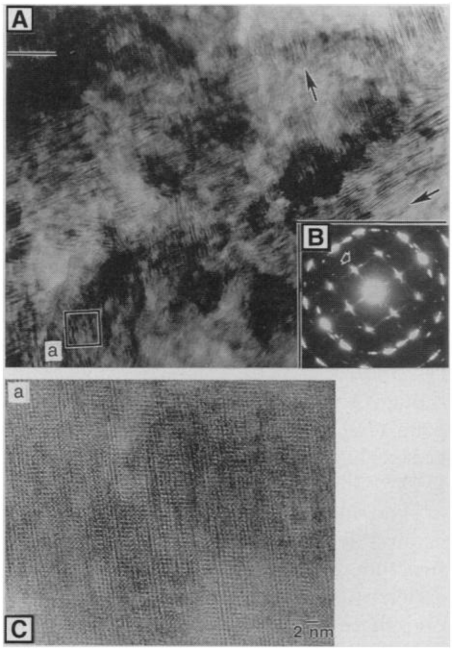

Fig. 3. VPO reduced in butane. (**A**) Two sets of extended defects (arrowed) parallel to [201] and the symmetry-related $[20\bar{1}]$ directions in (010) orientation in diffraction contrast (~400°C, several hours). (**B**) The electron diffraction pattern reveals two sets of diffuse streaks along these directions. (**C**) One set of the defects in HREM [from the area marked "a" in (A)].

by a pure shear mechanism, introducing the extended defects to reduce the misfit between the reduced surface layers containing anion vacancies (which change the strength of the Lewis acid sites) and the underlying matrix (Fig. 1D). At the fault boundary (Fig. 1B), the structure is preserved as before, and the displacements at the idealized faults do not lead to a change in the stoichiometry. The result is a disordered (polytype of) VPO with defective and unreduced matrix regions differing only in local symmetry.

The increased defect concentration found with increased reduction indicates the creation and diffusion of more anion vacancies. The repeated glide shear with increased reduction can lead to ordering of these pure shear defects (as in the case of CS planes), to a lower energy (201) face, eventually forming an ordered, anion-deficient phase. Indeed, evidence for such a phase is obtained in samples after prolonged reduction, as shown in the electron diffraction pattern in Fig. 5. The superstructure suggests that equilibrium is reached in a few days. The observation of two sets of defects suggests that the two twin (symmetry-related) orientations contribute to the superlattice. The energy requirement for the glide defect mechanism proposed here is much less than that for a CS plane, which eliminates crystal lattice sites and causes lattice collapse.

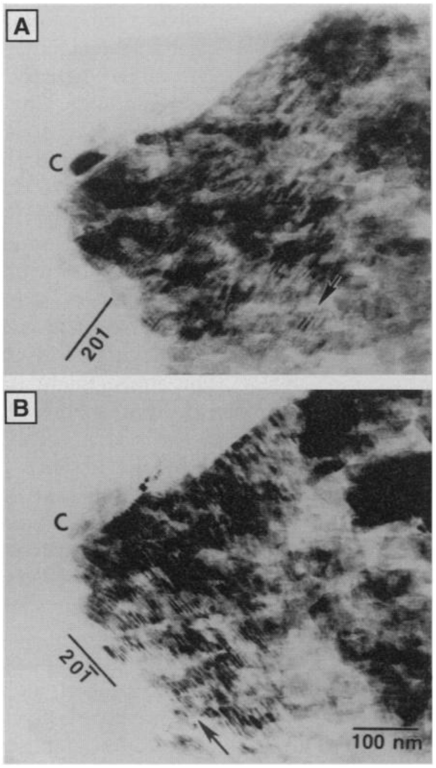

Fig. 4. Diffraction contrast in (**A**) 201 and (**B**) $20\bar{1}$ reflections from the same area near c reveals that the displacement vector (**R**) lies in the plane of shear {201}, indicating a pure (glide) shear mechanism. In diffraction contrast defect analysis, for example, the planar defect parallel to [201] was present in the 201 reflection but was invisible in $20\bar{1}$, 010 reflections.

The growth and ordering of the extended defects into an anion-deficient phase could eventually reduce the number of active basal sites in the lattice. By measuring the defect density per unit cell, one can estimate the local anion deficiency in defective regions. The defects described here have an almost pure shear (screw) character, and they can be nucleated as small shear loops in the presence of large shear strains arising because of structural modifications during catalysis. The loops can expand through a glide mechanism that is driven by lattice strain. After reduction for a few days, on average, one line defect per $\sim$7 unit cells was observed. This value would indicate an anion deficiency associated with the extended defects in the sample of $\sim$0.15, giving a V oxidation state of $\sim$3.7. The defective phase corresponds to $(VO)_2P_2O_{6.67}$. These estimates may relate only to the vacancy supersaturation, and there will be some background concentration of point defects in the catalyst.

Cevani *et al.* (*13*) and Centi (*6*) observed an increased activity in butane-MA in VPO catalysts prepared by the organic route and attributed it to the presence of disorder along the (020) cleavage planes. These investigations postulated that, in order to activate *n*-butane selectively, the presence of suitable neighboring sites would be necessary for simultaneous interaction: One center would need to be able to abstract a hydrogen atom, and one center would need to be able to accommodate excess electrons from the alkane. They suggested that the disorder might derive from defects from two neighboring (edge-sharing) V atoms in the active plane, one with an apical (nonplanar) oxygen vacancy on top of one V (shown as site 1 in Fig. 1E) from inversion from a trans to a cis vanadyl position, or from modifications in the V–O bond strength. However, evidence for the precise nature of the disorder was not clear from their x-ray diffraction measurements.

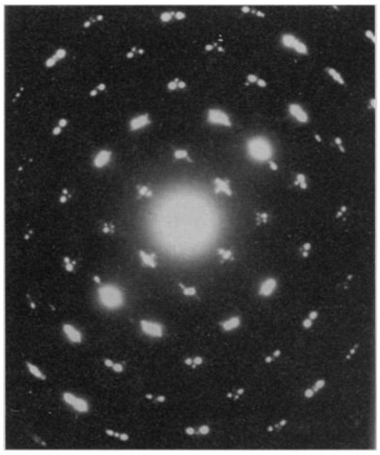

Fig. 5. Electron diffraction pattern showing a superlattice after reduction for a few days.

On the basis of our EM results of defect structures, we believe that, during the initial stages of the reduction, anion vacancies are formed at the basal O sites connecting corner-sharing phosphate tetrahedra and the V octahedra (P–O–V) in the active plane (site 2 in Fig. 1E). The extended defects are introduced by a glide shear mechanism into the crystal to reduce the misfit between the reduced surface layers containing these anion vacancies and the underlying VPO matrix: The anion vacancies in the surface layers are associated with strong Lewis acid sites for dehydrogenation; they lower the local oxidation state of V and thus may lead to the formation of a highly reactive vanadyl (V–V) pair with an adjacent vacancy, capable of activating the alkane. Our proposal is also consistent with the fact that "activation" of the catalyst in a slightly reducing atmosphere is often necessary. Activation of the catalyst may generate the anion vacancies for alkane activation because the equilibrated (010) face is a stable surface.

REFERENCES AND NOTES

1. B. K. Hodnett, *Catal. Rev. Sic. Eng.* **27**, 373 (1985).
2. R. I. Bergman and N. W. Frisch, U.S. Patent 3,293,268 (1966).
3. R. L. Verma and L. D. Saraf, *Ind. Eng. Chem. Prod. Res. Dev.* **18**, 7 (1979).
4. E. Bordes, *Catal. Today* **1**, 499 (1987).
5. G. Centi *et al.*, *Chem. Rev.* **88**, 55 (1988).
6. G. Centi, *Catal. Today* **16**, 1 (1993); G. Centi, Ed., "Vanadyl Pyrophosphate Catalysts" [special issue, *Catal. Today* **16**, 1–153 (1993)].
7. D. Beltran-Porter *et al.*, *Eur. J. Solid State Inorg. Chem.* **28**, 131 (1991).
8. Y. E. Gorbunova and S. E. Linde, *Dokl. Akad. Nauk SSSR* **279**, 585 (1979).
9. H. Horowitz *et al.*, *Appl Catal.* **38**, 193 (1988).
10. M. Lopez Granados *et al.*, *J. Catal.* **112**, 671 (1993).
11. R. A. Schneider *et al.*, U.S. Patent 4,043,943 (1977).
12. F. Cevani *et al.*, *Appl. Catal.* **9**, 191 (1984).
13. F. Cevani, G. Centi, F. Triffiro, *J. Chem. Soc. Chem. Commun.* **107**, 7759 (1985).
14. J. Ebner and M. Thompson, in *Structure-Activity*, R. Grasselli and A. W. Sleight, Eds. (Elsevier, Amsterdam, 1991), pp. 31–37.
15. E. D. Boyes *et al.*, *Physica C* **159**, 801 (1989).
16. E. D. Boyes and P. L. Gai, *et al.*, unpublished results.
17. P. B. Hirsch *et al.*, *Electron Microscopy of Thin Crystals* (Krieger, Malabar, FL, 1985).
18. P. L. Gai and E. M. McCarron III, *Science* **247**, 553 (1990).
19. P. L. Gai-Boyes *et al.*, *J. Phys. Chem.* **96**, 8206 (1992).
20. P. L. Gai-Boyes, *Catal. Rev. Sci. Eng.* **34**, 1 (1992).
21. E. Bordes, *Catal. Today* **16**, 27 (1993).
22. We are grateful to L. G. Hanna, F. Gooding, and D. L. Smith for technical assistance. We thank R. Coulson, G. Sonnichsen, and H. Bergna for helpful discussions.

13 September 1994; accepted 5 December 1994